

Synthesis of Two-Dimensional Perovskite by Inverse Temperature Crystallization and Studies of Exciton States by Two-Photon Excitation Spectroscopy

Zhihui Chen, Qi Zhang, Menglong Zhu, Xinyun Wang, Qixing Wang, Andrew Thye Shen Wee, Kian Ping Loh, Goki Eda,* and Qing-Hua Xu*

Two-dimensional (2D) organic–inorganic hybrid perovskites (OIHPs), a natural multiple-quantum-well structure with quasi-2D electronic properties, have recently emerged as a promising class of semiconducting materials for photovoltaic and optoelectronic applications. However, facile synthesis of high-quality 2D OIHPs single crystals is still lacking. The layer dependence of the exciton binding energy of $(\text{C}_4\text{H}_9\text{NH}_3)_2\text{PbI}_4$ (C4PI), a widely studied 2D OIHP, is still debated. Herein, a novel synthesis technique based on inverse temperature crystallization in a binary-solvent system is used to prepare 2D OIHPs and a systematic study of excitonic states of the synthesized 2D OIHPs by two-photon excitation (TPE) spectroscopy is conducted. The obtained TPE spectra indicate that the exciton binding energies are similar for C4PI nanosheets and bulk crystals with different number of layers, most likely due to the intrinsically weak interlayer coupling. Further, the dark excitonic $2p$ states of $(\text{C}_6\text{H}_5(\text{CH}_2)_2\text{NH}_3)_2\text{PbI}_4$ (PEPI) and C4PI are also observed by TPE spectroscopy. The results provide a novel synthesis protocol and insight into exciton properties of 2D OIHPs.

OIHPs have ABX_3 three-dimensional (3D) lattice frameworks, where A represents small-sized organic cation (CH_3NH_3^+ , $\text{CH}(\text{NH}_2)_2^+$, Cs^+ , $\text{CH}_3(\text{NH}_2)_2^+$), B represents bivalent metal cation (Pb^{2+} , Sn^{2+} , Ge^{2+}), and X is a halogen anion (Cl^- , Br^- , I^-). In addition to the cubic 3D structure, precursors of OIHPs can assemble into a van der Waals layered A_2BX_4 structure where the large-sized organic moieties separate the corner-shared BX_6^{4-} octahedra inorganic layers (see Figure 1a).^[7–10] As the band gap of the organic layers is much larger than that of the inorganic layers,^[11] the organic molecules electronically isolate the inorganic layers to form multiple-quantum-well structure,^[12–19] which is responsible for the observation of thickness independent band gap of 2D perovskites in some studies.

Similar to graphene and its inorganic analogues such as transition metal dichalcogenides (TMDs), electronic and optical properties of 2D OIHPs are very different from their 3D counterparts.^[14,20,21] Due to strong Coulombic interactions in the electron-hole pair, 2D OIHPs generally exhibit strong excitonic absorption and emission. The exciton binding energy (E_b) can be determined by measuring the energy difference between the ground excitonic state (E_{1s}) and electronic band gap (E_g).^[22–25] The exciton binding energy is generally sensitive to dielectric environment, ranging from tens to hundreds of meV.^[26–28] In order to study the excitonic properties of the 2D OIHPs as well as integration with other 2D materials to achieve novel functionalities, it is important to understand layer-dependent excitonic properties, especially exciton binding energy, which is critical for device performance.^[29–31]

There are several reports on investigation of exciton binding energy of 2D OIHPs.^[12,13,16,17,32] The understanding of the exciton binding energy in these 2D systems still remains controversial. It was previously reported that exciton binding energy of mechanically exfoliated bilayer $(\text{C}_4\text{H}_9\text{NH}_3)_2\text{PbI}_4$ (C4PI) crystals (≈ 490 meV) was significantly larger than that of the corresponding C4PI bulk material (≈ 360 meV).^[13] This result suggests that their electronic properties are strongly influenced not only by the adjoining insulating organic ligands but also by their surrounding dielectric medium. However, a recent work by Zhang et al. showed that exciton binding energies of

1. Introduction

Organic–inorganic hybrid perovskites (OIHPs) have emerged as a promising platform for photovoltaic and optoelectronic device applications owing to their long carrier diffusion lengths, large absorption coefficients, and defects tolerance.^[1–6]

Dr. Z. H. Chen, Dr. M. L. Zhu, Prof. K. P. Loh, Prof. Q.-H. Xu
Department of Chemistry
National University of Singapore
3 Science Drive 3, Singapore 117543, Singapore
E-mail: chmxqh@nus.edu.sg

Dr. Q. Zhang, X. Y. Wang, Dr. Q. X. Wang, Prof. A. T. S. Wee, Prof. G. Eda
Department of Physics
National University of Singapore
2 Science Drive 3, Singapore 117542, Singapore
E-mail: g.eda@nus.edu.sg

Dr. M. L. Zhu, Prof. A. T. S. Wee, Prof. K. P. Loh, Prof. Q.-H. Xu
SZU-NUS Collaborative Innovation Center and International
Collaborative Laboratory of 2D Materials for Optoelectronics Science
and Technology of Ministry of Education
Institute of Microscale Optoelectronics
Shenzhen University
Shenzhen 518060, China

 The ORCID identification number(s) for the author(s) of this article can be found under <https://doi.org/10.1002/adfm.202002661>.

DOI: 10.1002/adfm.202002661

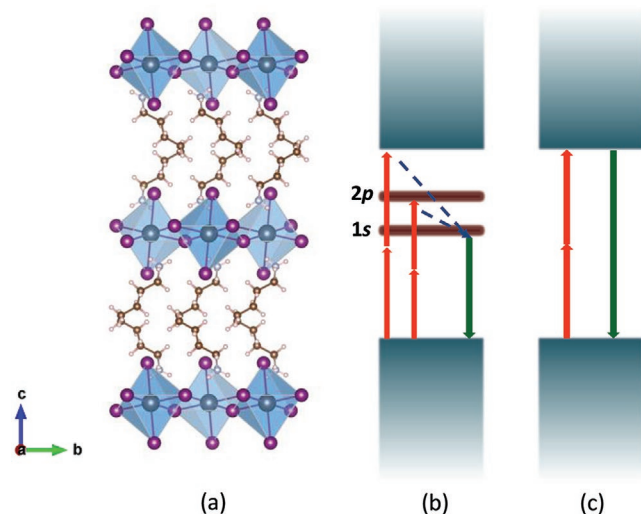


Figure 1. a) The atomic structure of C4PI. Black, purple, brown, light grey, and pink balls represent Pb, I, C, N, and H atoms. Schematic of the optical band structure, showing the two-photon absorption (red arrows) and fluorescence emission (green arrows) processes in an excitonic and a non-excitonic system, respectively. b) In the exciton picture, the excitonic 1s state is not accessible under two-photon excitation, while the 2p and continuum states are excited. The fluorescence emissions still generate from 1s state following the Kasha's rule. c) In the band picture, the onset for two-photon absorption occurs at the band edge, where the fluorescence emission also happens.

both $(C_6H_5(CH_2)_2NH_3)_2PbI_4$ (PEPI) and C4PI of different thicknesses, ≈ 3 layers and ≥ 20 layers, were both ≈ 200 and ≈ 250 meV, that is, weakly sensitive to the number of layers.^[33]

Single crystal is a preferred form for investigating intrinsic physical properties of OIHPs because grain boundaries in polycrystalline systems obscure optical features, making detailed analysis difficult. Various protocols have been proposed to synthesize single crystals of OIHPs, including hot solution cooling-induced crystallization,^[34] seed-assisted crystallization,^[35,36] and anti-solvent-induced crystallization,^[37,38] whereas these three methods are time-consuming. A novel method based on retrograde solubility (i.e., lower precursor solubility at higher temperature) was recently employed to synthesize high-quality 3D OIHPs single crystals within minutes, which is cost-effective and convenient.^[39] This synthesis technique, known as the inverse temperature crystallization, can be potentially extended to the preparation of 2D OIHPs. However, this has not been demonstrated to date.

In this work, single crystals of C4PI were prepared through the inverse temperature crystallization method, and their excitonic states were probed by two-photon excitation (TPE) spectroscopy. Complementary to the conventional one-photon excitation process that allows access to the final states with even parity (1s, 2s, 3s), two-photon excitation allows access to final states with odd parity such as 2p, 3p states (see Figure 1b).^[40–42] These states with odd parity are generally known as “dark” states and do not appear in the linear absorption spectrum. TPE spectroscopy is a powerful tool for studying excitonic effects because of enhanced resonance features and weak sensitivity to disorder effects.^[22] In the system where the excitonic effects are negligible, the onset of two-photon absorption is expected to be consistent with that of one-photon absorption as illustrated

in Figure 1c. On the other hand, in excitonic systems, TPE spectrum can distinguish discrete dark states and continuum states. TPE spectroscopy has been utilized to study excitonic states in bulk materials such as GaAs,^[43] 2D materials such as TMDs,^[22,44] and 1D materials such as single-walled carbon nanotube.^[45] Here, TPE spectroscopy was utilized to probe the excitonic states of chemically synthesized C4PI single crystals.

2. Results and Discussion

Bulk single crystals of C4PI were synthesized in a binary solvent system through an inverse temperature crystallization method. Figure 2a shows the schematic illustration of the synthetic process (see detailed synthetic conditions in the Experimental Section). Precursors (lead iodide and ammonium salt) with stoichiometric ratio were first dissolved in *N,N*-dimethylformamide (DMF) at room temperature. Dropwise addition of toluene, as anti-solvent, into this solution resulted in precipitation of yellowish solids, which were ascribed to semi-amorphous crystallites of 2D perovskite (Figure S1a, Supporting Information). These crystallites showed retrograde solubility behavior and could be redissolved in the binary solution at temperatures below ≈ -20 °C (Figure S1b, Supporting Information). Single crystals of 2D OIHPs were then formed as the temperature of precursor solution increased (see Videos S1 and S2, Supporting Information). With this method, single crystals were prepared at a growth temperature ranging from 40 to 120 °C. The average size of the prepared crystal is inversely correlated to the growth temperature, indicating that the nucleation rate is greater than crystal growth rate at higher temperatures. Optical images of the obtained crystals at a growth temperature of 40 °C (Figure S2, Supporting Information) show that the crystal size can reach to millimeter scale, which is comparable to that of slow-growth methods.^[35,36,38] The stoichiometry of the crystals obtained from electron dispersive spectroscopy (EDS) measurements agrees well with the theoretical value for C4PI and PEPI (Figure S3, Supporting Information). Powder X-ray diffraction spectrum shows sharp peaks, suggesting their high crystallinity (Figure S4, Supporting Information). Atomic force microscopy (AFM) results show that the typical thickness of bulk C4PI crystals was around 2.4 μm (Figure 2c,d). Bulk C4PI crystal exhibits a broad absorption band with a maximum at ≈ 510 nm and a tail stretching up to 700 nm. Photoluminescence (PL) spectrum of the crystal at room temperature shows an intense excitonic peak centered at ≈ 523 nm, a common feature of 2D OIHPs (Figure 2h).^[12]

C4PI nanosheets were prepared by mechanical exfoliation of C4PI bulk crystal onto the surface of a quartz substrate. Chemically inert hexagonal boron nitride (h-BN) was used as a protective capping layer of C4PI nanosheets to prevent them from degradation in ambient condition. A multilayer h-BN was first exfoliated onto a polydimethylsiloxane (PDMS) film^[40] and then transferred onto the C4PI nanosheets, forming a C4PI/h-BN heterostructure (Figure 2e). AFM measurements indicate that the thickness of the C4PI nanosheets was ≈ 7.68 nm, corresponding to 5 layers of C4PI (Figure 2f,g).^[46,47] Compared to the bulk crystals, the absorption peak of C4PI nanosheets (≈ 513 nm) is significantly narrower. The corresponding PL peak occurs at ≈ 517 nm. The Stokes shift of nanosheet is ≈ 20 meV, which is distinctly smaller than that of bulk sample

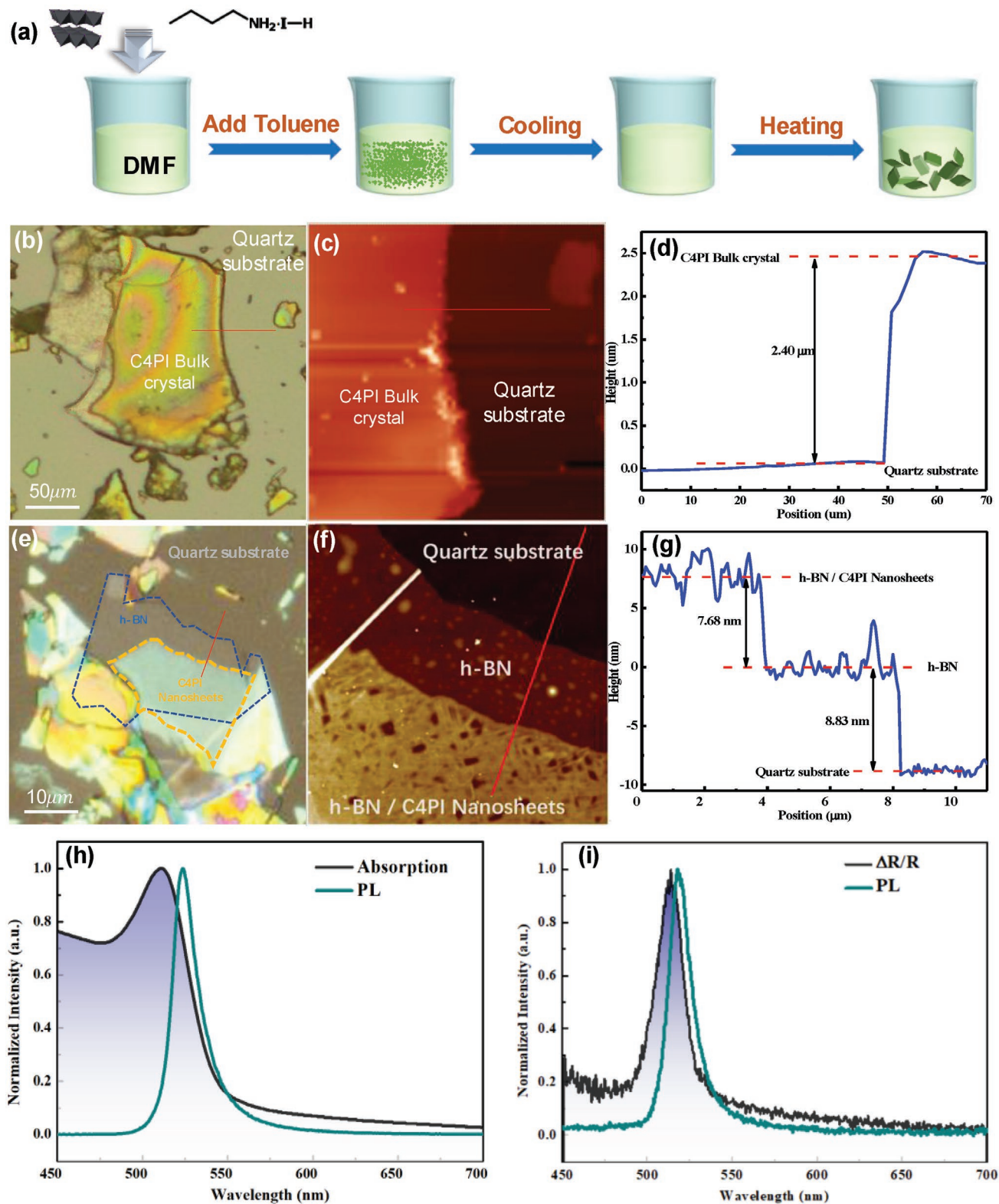


Figure 2. a) Schematic procedures for synthesis of C4PI bulk crystal. b) Optical image for C4PI bulk crystal. c,d) AFM topography and height profile of C4PI bulk crystal. e) Optical image for C4PI nanosheet. The region circled by blue dash line represents multilayer h-BN, while orange region outlines C4PI nanosheets. f,g) AFM topography and height profile of C4PI nanosheet on quartz substrate. The height profiles were tracked along the red lines. h) Absorption and PL spectrum of C4PI bulk crystal at room temperature ($\lambda_{\text{exc}} = 473\text{ nm}$). i) Differential reflectance (DR) and PL spectrum of C4PI nanosheets at room temperature ($\lambda_{\text{exc}} = 473\text{ nm}$). The scale bars of optical images are shown in panels.

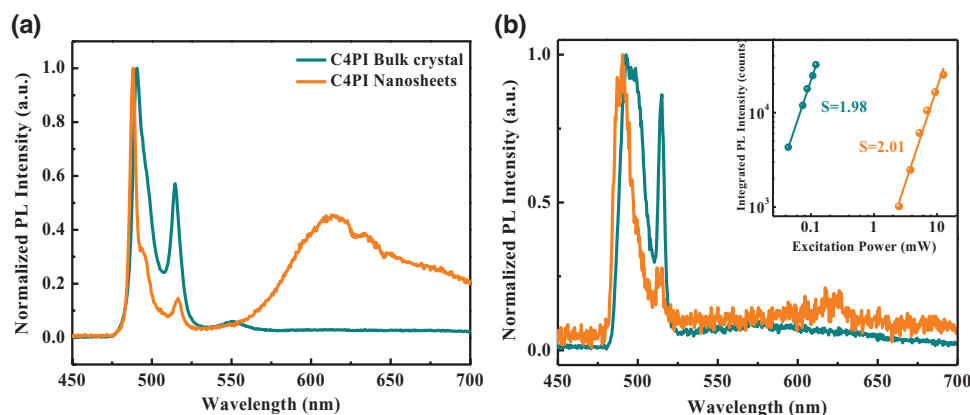


Figure 3. a) PL spectrum of C4PI bulk crystal (dark cyan line) and C4PI nanosheets (orange line) ($\lambda_{\text{EXC}} = 473$ nm) under 78 K. b) Main panel: TPPL emission spectrum of C4PI bulk crystal (dark cyan line) and C4PI nanosheets (orange line) ($\lambda_{\text{EXC}} = 890$ nm) under 78 K. Inset: the power dependence TPPL at 490 nm. PL intensities exhibit quadratic power dependence on the excitation power range, confirming the two-photon excitation nature of the fluorescence.

(≈ 60 meV; Figure 2h,i). The narrow bandwidth of absorption and PL peak is comparable to those reported for single crystals prepared by other methods, suggesting that the crystal quality of our synthesized material is comparably high.^[13]

In order to reduce the thermal broadening effect,^[22,48] PL spectrum of the 2D perovskites was also measured at 78 K. PL spectra of both bulk crystals and nanosheets at 78 K show three emission bands (Figure 3a). The resonance peak at 515 nm can be ascribed to the room temperature (RT) phase, while the peak at 490 nm is related to the low temperature (LT) phase. These two phases are structurally different with different degrees of interface strain between the alkylammonium chains.^[26,27] The additional broadband emission is due to mid-gap defect states.^[11]

TPE and two-photon PL (TPPL) spectra were both measured by using femtosecond laser pulses as the excitation source. The experimental setup is shown in the supporting information (Figure S5, Supporting Information). TPPL spectra of C4PI nanosheets and bulk crystals at 78 K (Figure 3b) show similar excitonic emissions to their corresponding one-photon-excitation PL spectrum. However, the broadband emission contribution to one-photon excitation PL spectra of C4PI nanosheets decreases significantly under two-photon excitation (Figure 3). The broadband emission in 2D OIHPs was attributed to the emission of the defect states,^[13] which is sensitive to the surface of the sample. Under two-photon excitation, the focal point may not be the same with that of one-photon excitation, resulting in different contributions of broadband emission under two situations. Two-photon excitation nature of the observed emission is confirmed by its quadratic power dependences on the excitation power (Figure 3b inset). Within the excitation power range, no saturation effects in TPPL were observed, which precludes the effects of ground state depletion^[49] or exciton–exciton annihilation.^[50,51]

TPE spectrum of C4PI at 78 K was measured by monitoring the emission intensity of the dominant low temperature phase peak at 490 nm under excitation at different wavelengths and normalizing the TPPL intensities with the corresponding excitation power (Figure 4a). TPE spectrum of PEPI bulk crystal was measured under the same experimental condition as a control sample.^[12,17] TPE resonance peaks of both C4PI bulk crystal

and nanosheets at 78 K are found at 2.9 eV. The resonance is attributed to the secondary absorption above the absorption edge region, which is believed associated with long-lived excitonic state trapped in the strong electrostatic field induced by the localized $(\text{C}_4\text{H}_9\text{NH}_3)^+$ ions around the PbI_4^- layers.^[7,52] At the lower energy side of the resonance peak, TPPL intensities of all three samples increase linearly with the excitation photon energy, which is the signature of two-photon absorption above the band edge in 2D systems excited with in-plane polarization.^[44] TPE spectra for PEPI and C4PI bulk crystals were also measured at 295 K for comparison (Figure S7, Supporting Information). However, the feature of linearly increased TPPL intensities with the excitation energy at 295 K is not very distinctive as a result of the broadening effects that smear the band edge at room temperature.^[48] The energy of the band edge, which was determined by extrapolation of the linear absorption edge (Figure 4a), is: 2.57 eV for PEPI bulk crystal, 2.77 eV for C4PI bulk crystal, and 2.74 eV for C4PI nanosheets. Moreover, the energy of 1s state (E_{1s}) was determined from the peak of TPPL spectra at 78 K with the addition of Stokes shift. For C4PI and PEPI, the Stokes shift is temperature independent due to the polaron origin of the emission line.^[13,53] As a result, E_{1s} energy was 2.41 eV for PEPI, 2.59 eV for C4PI bulk crystal, and 2.55 eV for C4PI nanosheets. The exciton binding energies ($E_b = E_g - E_{1s}$) are therefore determined to be 160 meV for PEPI bulk crystal, 180 meV for C4PI bulk crystal, and 190 meV for C4PI nanosheets, respectively. The measured values of the electronic band gap and the exciton binding energy of the PEPI bulk crystal agree with the previously reported results,^[4,10] which verifies the reliability of the TPE spectroscopy method and the measurement system as an effective tool to probe the excitonic states of these materials. Note that the TPE spectrum of room temperature phase yields similar results (Figure S8, Supporting Information). Meanwhile, E_g values were also obtained by fitting the linear absorption spectrum near the band edge using Elliott's model (Figure S9, Supporting Information).^[54] For C4PI nanosheet, the obtained E_g value according to Elliott's model matches well with that of TPE spectroscopy (Table S1, Supporting Information). The deviations of E_g values for C4PI and PEPI bulk crystals may be due to the ensemble absorption measurements (UV–vis spectroscopy). The presence of surface and edge

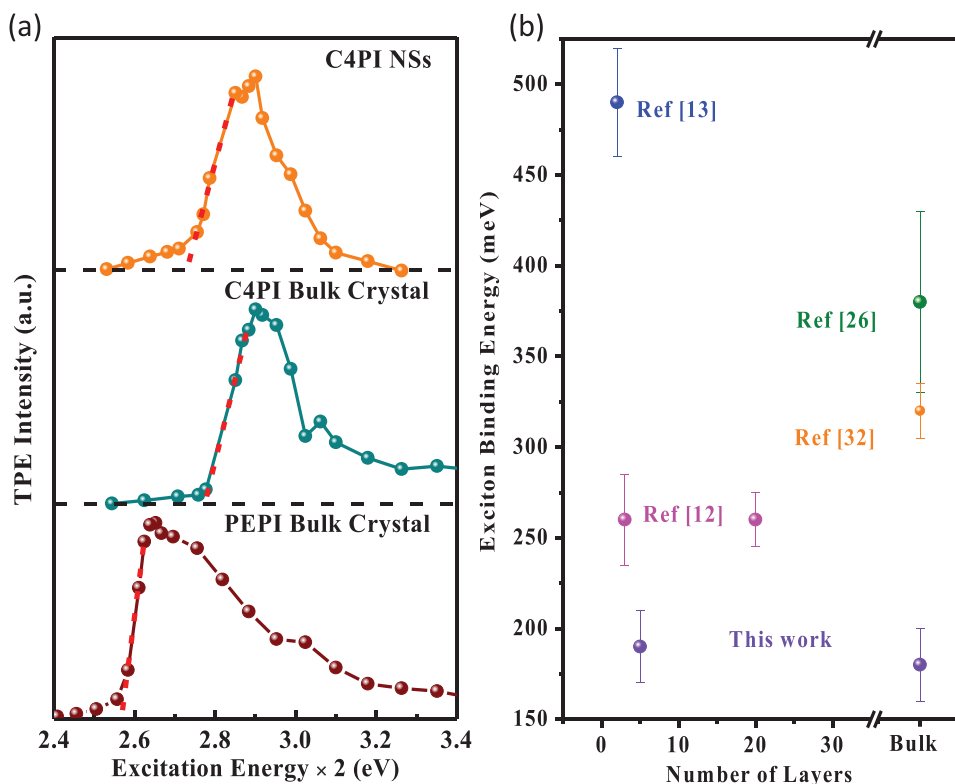


Figure 4. a) TPE spectrum of C4PI nanosheets, C4PI bulk crystal and PEPI bulk crystal at 78 K. The intercepts of the red dash lines indicate the electronic band edge of the samples. b) Summary of exciton binding energies of C4PI with different thicknesses.

states of the bulk crystals may alter and broaden the absorption spectrum, which induces the deviation from the intrinsic excitonic and continuum absorption of bulk crystals.

Figure 4b summarizes the exciton binding energies of C4PI measured in this work and those of previous reports. The exciton binding energy is determined by the difference between absorption edge and 1s state. As the individual excitonic layers are electronically isolated in 2D OIHPs due to the insulating organic layers, the band gap of C4PI is expected to be insensitive to the number of layers, unlike the case of TMDs.^[55] However, E_{1s} could be affected by environmental dielectric effects, reorganization of the organic ligands and strain in the thin layer limit.^[9,13,14,31] Here, the exciton binding energies obtained from nanosheets and bulk crystal are both around 185 meV, indicating that these effects do not play a dominant role for crystals thicker than five layers.

Dark excitonic states such as $2p$ states can be probed using TPE spectroscopy by scanning the excitation wavelength within the sub-band-gap energy range.^[22] The $2p$ state is the lowest lying symmetry-allowed state for the two-photon excitation process and a corresponding resonance peak appears in the TPE spectrum.^[22] Figure 5a shows high resolution TPE spectra of the OIHP crystals near the band edge region. We observe a weak resonance feature on top of the band edge absorption tail in this spectral range. Their energy values relative to that of the ground exciton state and electronic band gap suggest that they arise from $2p$ exciton resonance. Optical absorption close to the edge (e.g., 1s and $2p$ excitons) in semiconductors can be examined by band theory together with the effective-mass approximation for the excitons.^[56] In direct band gap semiconductors, the

oscillator strength is nonzero only for s states and falls like n^{-3} and becomes continuum as the absorption edge is approached. The oscillator strength per atom of 1s state is generally on the order of (atomic radius/exciton radius)³ per atom. For 2D OIHPs, atomic radius is ≈ 1.4 Å for iodine and ≈ 1.8 Å for Pb atom. The exciton radius is comparable to the unit cell size of ≈ 20 – 50 Å.^[57] Under two-photon excitation, excitonic resonance will lead to an enhancement near the band edge, analogous to the results for one-photon excitation.^[45] The relative contribution of $2p$ state relative to that of the continuum of the band edge is expected to be one order of magnitude smaller than that of one-photon absorption spectrum. The weak $2p$ resonance was also observed in $(C_4H_9NH_3)_2PbBr_4$ 2D perovskite.^[16]

In 2D hydrogenic model, exciton binding energy is described by $E_{b(n)} = R_y \frac{\mu}{\epsilon^2 (n-0.5)^2}$, where n is principle quantum number, R_y is Rydberg constant, μ is exciton effective mass, and ϵ is dielectric constant. Binding energies of 1s and $2p$ excitons are $E_{b(1s)} = R_y \frac{4\mu}{\epsilon^2}$ and $E_{b(2p)} = R_y \frac{4\mu}{9\epsilon^2}$. The energy difference between 1s and $2p$ excitons could be utilized to estimate exciton binding energy: $E_b = E_g - E_{1s} = E_{b(1s)} = \frac{9}{8} (E_{b(1s)} - E_{b(2p)}) = \frac{9}{8} (E_{2p} - E_{1s})$. Energy levels of 1s, $2p$ resonance and electronic band gap of PEPI and C4PI are summarized in Figure 5b. The exciton binding energies of PEPI and C4PI (bulk crystal/nanosheets) are estimated to be 146 and 158/152 meV from energy difference between 1s and $2p$ resonance. The estimated exciton binding energies according to the 2D hydrogenic model are a little bit smaller than experimentally measured results for PEPI and C4PI (bulk crystal/nanosheets). These deviations of exciton binding

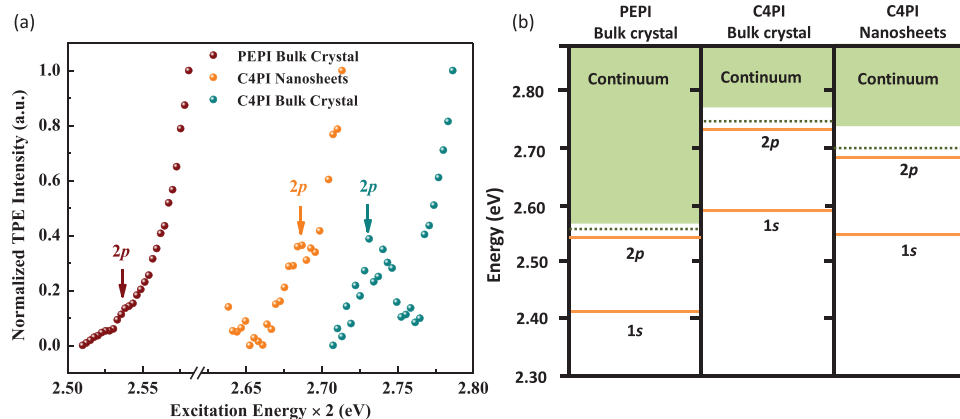


Figure 5. a) TPE spectrum of C4PI nanosheets, C4PI bulk crystal and PEPI bulk crystal at 78 K in sub-band-gap energy range. b) Exciton excitation spectrum of PEPI, C4PI bulk crystal and C4PI nanosheets determined experimentally in this work compared with the 2D hydrogenic model. Orange lines denote the one-photon active 1s states and two-photon active 2p states. Green rectangles represent the continuum states. Dark green dash lines denote the estimated band edges according to the 2D hydrogenic model.

energies could arise from the existence of image charge effect in 2D OIHPS.^[58]

3. Conclusion

In summary, we have demonstrated a novel synthesis method of 2D OIHPS using the inverse temperature crystallization and investigated their excitonic properties. At 78K, same TPPL emission peak wavelengths and similar Stokes shifts were obtained for C4PI nanosheets and bulk crystal, suggesting similar E_{1s} energies for them. Furthermore, TPE spectroscopy was utilized to determine the electronic band edge of the 2D OIHPS. Interestingly, we found that the exciton binding energies of C4PI are similar for 5-layer and bulk crystals, despite their different number of layers. This is most likely due to the isolated electronic structure of the organic–inorganic quantum-well structure and weak interlayer coupling in both 2D OIHPS bulk crystals and nanosheets. Moreover, we observed the 2p states of 2D OIHPS, from which we verified the consistency in the exciton binding energy of these materials.

4. Experimental Section

Chemicals and Reagents: Phenethylamine ($\geq 99\%$), *n*-butylamine ($\geq 99\%$), toluene (ACS reagent, $\geq 99.5\%$), ethanol (ACS reagent, $\geq 99.5\%$), *N,N*-dimethylformamide (ACS reagent, $\geq 99.8\%$), lead (II) iodide (99%), hydroiodic acid (57 wt%) were purchased from Sigma Aldrich. All chemicals were used as received without any further purification.

Synthesis of Ammonium Salts $C_6H_5(C_2H_4)NH_3I$ (PEI) and $C_4H_9NH_3I$ (C4I): Ethanol (10 mL) and phenethylamine (2.52 mL) ($C_6H_5(C_2H_4)NH_2$) were mixed in a beaker and kept at 0 °C under an ice bath. Stoichiometric amount of HI (a.q. 2.62 mL) was added to the mixture dropwise under stirring. The stirring continued for 2 h to ensure complete reaction. The solution was heated up to 50 °C with a rotary evaporator to remove the solvent until whitish ammonium salt powder appeared. The ammonium salt powder was collected and washed with diethyl ether three times and then transferred to a vacuum oven to dry at 60 °C for 24 h for later use. A similar process was utilized to synthesis of C4I by using *n*-butylamine as the precursor solvent instead.

Inverse Temperature Crystallization of PEPI: Stoichiometric amount of PEI and PbI_2 was dissolved in DMF to prepare 0.1 M precursor solution. Seven milliliters of toluene was added dropwise to 0.2 mL the precursor solution in a vessel and PEPI semi-amorphous crystallites would precipitate out from the mixture. The mixture was stored in a freezer at ≈ -20 °C until the crystallites redissolve in the solution and then PEPI single crystal will grow upon heating the vessel at 80 °C.

Inverse Temperature Crystallization of C4PI: Stoichiometric amount of C4I and PbI_2 was dissolved in DMF to prepare 0.2 M precursor solution. Eight milliliters of toluene was added dropwise to 0.2 mL precursor solution in a vessel and C4PI crystallites would precipitate out from the mixture. The mixture was put in a freezer at ≈ -20 °C until the crystallites redissolve in the solution and then C4PI single crystal will grow upon heating the vessel at 80 °C.

Energy Dispersive Spectroscopy (EDS) and Scanning Electron Microscope (SEM) Characterizations: EDS results were obtained by using the JEOL JSM6700-F SEM mode, with the Oxford Instruments X-MaxN 150 EDS detector. Silicon substrate was made to stick to the sample holder with a carbon tape to improve conduction. Measurements were conducted in high vacuum at $\approx 7 \times 10^{-7}$ Torr with beam voltage 5 and 15 kV for SEM and EDS, respectively. Beam current was 10 μA for both characterizations.

Powder X-Ray Diffraction (PXRD) Measurement: The PXRD experiments were performed in transmission mode with a Bruker D8 Advance A25 diffractometer equipped with graphite monochromated Cu $K\alpha$ radiation ($\lambda = 1.54073 \text{ \AA}$) at room temperature.

Atomic Force Microscopy (AFM) Measurement: AFM (Bruker Dimension FastScan, Tapping mode) was used to measure height profile of the exfoliated C4PI bulk crystal and nanosheets.

Linear Optical Measurements: Bright field and fluorescence images were taken using optical microscope (Olympus, BX51TR). Absorbance spectra were obtained by UV–vis–NIR spectrophotometer (Shimadzu UV-2600). Micro-PL spectra were obtained with a laser confocal microscope (NT-MDT, NTEGR Spectra) in back scattering geometry with a 473 nm (continuous wave) excitation.

TPE Spectroscopy: The laser beam with a pulse duration of ≈ 140 fs and a repetition rate of 80 MHz from a femtosecond mode-locked Ti: sapphire laser (Chameleon Ultra II, Coherent) acted as the excitation source. The laser beam was first cleaned by passing through a long pass filter (with a cutoff wavelength of 715 nm) and then reflected by a 50/50 beam splitter into the objective lens (10 \times , NA = 0.3) to focus onto the sample. The samples were loaded in to a Linkam stage (THMS600) for temperature control. The same objective lens was utilized to collect the TPPL signals. Their spectra were measured by a monochromator (Acton, Spectra Pro 2300i) coupled CCD (Princeton Instruments, Pixis 100B).

Supporting Information

Supporting Information is available from the Wiley Online Library or from the author.

Acknowledgements

Z.H.C., Q.Z., and M.L.Z. contributed equally to this work. This work is financially supported by Ministry of Education, Singapore (Tier 1 R-143-000-A41-114, Tier 2 MOE2018-T2-1-119, and Tier 3 MOE2018-T3-1-005).

Conflict of Interest

The authors declare no conflict of interest.

Keywords

dark excitonic states, exciton binding energy, multiple-quantum-well structure, two-dimensional organic–inorganic hybrid perovskites, two-photon excitation

Received: March 24, 2020

Revised: April 29, 2020

Published online:

- [1] J. Huang, Y. Yuan, Y. Shao, Y. Yan, *Nat. Rev. Mater.* **2017**, *2*, 17042.
- [2] Y.-H. Kim, H. Cho, J. H. Heo, T.-S. Kim, N. Myoung, C.-L. Lee, S. H. Im, T.-W. Lee, *Adv. Mater.* **2015**, *27*, 1248.
- [3] Y. Yuan, T. Li, Q. Wang, J. Xing, A. Gruverman, J. Huang, *Sci. Adv.* **2017**, *3*, e1602164.
- [4] Q. Sun, J. Wang, W.-J. Yin, Y. Yan, *Adv. Mater.* **2018**, *30*, 1705901.
- [5] J. Burschka, N. Pellet, S.-J. Moon, R. Humphry-Baker, P. Gao, M. K. Nazeeruddin, M. Grätzel, *Nature* **2013**, *499*, 316.
- [6] A. Kojima, K. Teshima, Y. Shirai, T. Miyasaka, *J. Am. Chem. Soc.* **2009**, *131*, 6050.
- [7] C. C. Stoumpos, D. H. Cao, D. J. Clark, J. Young, J. M. Rondinelli, J. I. Jang, J. T. Hupp, M. G. Kanatzidis, *Chem. Mater.* **2016**, *28*, 2852.
- [8] J.-C. Blancon, H. Tsai, W. Nie, C. C. Stoumpos, L. Pedesseau, C. Katan, M. Kepenekian, C. M. M. Soe, K. Appavoo, M. Y. Sfeir, S. Tretiak, P. M. Ajayan, M. G. Kanatzidis, J. Even, J. J. Crochet, A. D. Mohite, *Science* **2017**, *355*, 1288.
- [9] P. van der Put, *Recl. Trav. Chim. Pays-Bas* **1996**, *115*, 199.
- [10] M. Mączka, M. Ptak, A. Gągor, D. Stefańska, A. Sieradzki, *Chem. Mater.* **2019**, *31*, 8563.
- [11] H. Zahra, A. Hichri, S. Jaziri, *J. Appl. Phys.* **2017**, *122*, 015701.
- [12] Q. Zhang, L. Chu, F. Zhou, W. Ji, G. Eda, *Adv. Mater.* **2018**, *30*, 1704055.
- [13] O. Yaffe, A. Chernikov, Z. M. Norman, Y. Zhong, A. Velauthapillai, A. van der Zande, J. S. Owen, T. F. Heinz, *Phys. Rev. B* **2015**, *92*, 045414.
- [14] W. Niu, A. Eiden, G. Vijaya Prakash, J. J. Baumberg, *Appl. Phys. Lett.* **2014**, *104*, 171111.
- [15] G. C. Papavassiliou, *Mol. Cryst. Liq. Cryst. Sci. Technol., Sect. C* **1996**, *286*, 231.
- [16] K. Tanaka, T. Takahashi, T. Kondo, K. Umeda, K. Ema, T. Umebayashi, K. Asai, K. Uchida, N. Miura, *Jpn. J. Appl. Phys.* **2005**, *44*, 5923.
- [17] X. Hong, T. Ishihara, A. V. Nurmikko, *Phys. Rev. B* **1992**, *45*, 6961.
- [18] X. Hong, T. Ishihara, A. V. Nurmikko, *Solid State Commun.* **1992**, *84*, 657.
- [19] K. Tanaka, T. Takahashi, T. Kondo, T. Umebayashi, K. Asai, K. Ema, *Phys. Rev. B* **2005**, *71*, 045312.
- [20] R. Singh, P. Singh, G. Balasubramanian, ArXiv180701221 Cond-Mat **2018**.
- [21] M. Mączka, M. Ptak, A. Gągor, D. Stefańska, J. K. Zaręba, A. Sieradzki, *Chem. Mater.* **2020**, *32*, 1667.
- [22] Z. Ye, T. Cao, K. O'Brien, H. Zhu, X. Yin, Y. Wang, S. G. Louie, X. Zhang, *Nature* **2014**, *513*, 214.
- [23] G. Bastard, E. E. Mendez, L. L. Chang, L. Esaki, *Phys. Rev. B* **1982**, *26*, 1974.
- [24] A. Chernikov, T. C. Berkelbach, H. M. Hill, A. Rigosi, Y. Li, O. B. Aslan, D. R. Reichman, M. S. Hybertsen, T. F. Heinz, *Phys. Rev. Lett.* **2014**, *113*, 076802.
- [25] J. F. Muth, J. H. Lee, I. K. Shmagin, R. M. Kolbas, H. C. Casey Jr., B. P. Keller, U. K. Mishra, S. P. DenBaars, *Appl. Phys. Lett.* **1997**, *71*, 2572.
- [26] J.-C. Blancon, H. Tsai, W. Nie, C. C. Stoumpos, L. Pedesseau, C. Katan, M. Kepenekian, C. M. M. Soe, K. Appavoo, M. Y. Sfeir, *Science* **2017**, *355*, 1288.
- [27] J.-C. Blancon, A. V. Stier, H. Tsai, W. Nie, C. C. Stoumpos, B. Traoré, L. Pedesseau, M. Kepenekian, F. Katsutani, G. T. Noe, J. Kono, S. Tretiak, S. A. Crooker, C. Katan, M. G. Kanatzidis, J. J. Crochet, J. Even, A. D. Mohite, *Nat. Commun.* **2018**, *9*, 2254.
- [28] B. Cheng, T.-Y. Li, P. Maity, P.-C. Wei, D. Nordlund, K.-T. Ho, D.-H. Lien, C.-H. Lin, R.-Z. Liang, X. Miao, I. A. Ajia, J. Yin, D. Sokaras, A. Javey, I. S. Roqan, O. F. Mohammed, J.-H. He, *Commun. Phys.* **2018**, *1*, 80.
- [29] J. Jagielski, S. Kumar, W.-Y. Yu, C.-J. Shih, *J. Mater. Chem. C* **2017**, *5*, 5610.
- [30] B. Cheng, T.-Y. Li, P.-C. Wei, J. Yin, K.-T. Ho, J. R. D. Retamal, O. F. Mohammed, J.-H. He, *Nat. Commun.* **2018**, *9*, 5196.
- [31] K. Leng, I. Abdelwahab, I. Verzhbitskiy, M. Telychko, L. Chu, W. Fu, X. Chi, N. Guo, Z. Chen, Z. Chen, C. Zhang, Q.-H. Xu, J. Lu, M. Chhowalla, G. Eda, K. P. Loh, *Nat. Mater.* **2018**, *17*, 908.
- [32] T. Ishihara, J. Takahashi, T. Goto, *Phys. Rev. B* **1990**, *42*, 11099.
- [33] Q. Zhang, L. Chu, F. Zhou, W. Ji, G. Eda, *Adv. Mater.* **2018**, *30*, 1704055.
- [34] Y. Chen, M. He, J. Peng, Y. Sun, Z. Liang, *Adv. Sci.* **2016**, *3*, 1500392.
- [35] M. Li, S. Han, B. Teng, Y. Li, Y. Liu, X. Liu, J. Luo, M. Hong, Z. Sun, *Adv. Opt. Mater.* **2020**, *8*, 2000149.
- [36] C. Ge, W. Zhai, C. Tian, S. Zhao, T. Guo, S. Sun, W. Chen, G. Ran, *RSC Adv.* **2019**, *9*, 16779.
- [37] M. Konstantakou, D. Perganti, P. Falaras, T. Stergiopoulos, *Crystals* **2017**, *7*, 291.
- [38] F. Lédée, G. Trippé-Allard, H. Diab, A. Pierre, D. Garrot, J.-S. Lauret, E. Deleporte, *CrystEngComm* **2017**, *19*, 2598.
- [39] M. I. Saidaminov, A. L. Abdelhady, B. Murali, E. Alarousu, V. M. Burlakov, W. Peng, I. Dursun, L. Wang, Y. He, G. Maculan, A. Goriely, T. Wu, O. F. Mohammed, O. M. Bakr, *Nat. Commun.* **2015**, *6*, 7586.
- [40] A. M. Ellis, *J. Chem. Educ.* **1999**, *76*, 1291.
- [41] E. B. Barros, R. B. Capaz, A. Jorio, G. G. Samsonidze, A. G. Souza Filho, S. Ismail-Beigi, C. D. Spataru, S. G. Louie, G. Dresselhaus, M. S. Dresselhaus, *Phys. Rev. B* **2006**, *73*, 241406.
- [42] J. Xiao, Z. Ye, Y. Wang, H. Zhu, Y. Wang, X. Zhang, *Light: Sci. Appl.* **2015**, *4*, e366.
- [43] K. Tai, A. Mysyrowicz, R. J. Fischer, R. E. Slusher, A. Y. Cho, *Phys. Rev. Lett.* **1989**, *62*, 1784.
- [44] A. Shimizu, T. Ogawa, H. Sakaki, *Phys. Rev. B* **1992**, *45*, 11338.
- [45] F. Wang, G. Dukovic, L. E. Brus, T. F. Heinz, *Science* **2005**, *308*, 838.
- [46] L. Dou, A. B. Wong, Y. Yu, M. Lai, N. Kornierko, S. W. Eaton, A. Fu, C. G. Bischak, J. Ma, T. Ding, *Science* **2015**, *349*, 1518.
- [47] L. Ma, J. Dai, X. C. Zeng, *Adv. Energy Mater.* **2017**, *7*, 1601731.
- [48] G. Zhang, A. Chaves, S. Huang, F. Wang, Q. Xing, T. Low, H. Yan, *Sci. Adv.* **2018**, *4*, eaap9977.
- [49] N. Dong, Y. Li, S. Zhang, N. McEvoy, R. Gatensby, G. S. Duesberg, J. Wang, *ACS Photonics* **2018**, *5*, 1558.

- [50] N. Kumar, Q. Cui, F. Ceballos, D. He, Y. Wang, H. Zhao, *Phys. Rev. B* **2014**, *89*, 125427.
- [51] Y. Ye, Z. Ye, M. Gharghi, H. Zhu, M. Zhao, Y. Wang, X. Yin, X. Zhang, *Appl. Phys. Lett.* **2014**, *104*, 193508.
- [52] D. H. Cao, C. C. Stoumpos, O. K. Farha, J. T. Hupp, M. G. Kanatzidis, *J. Am. Chem. Soc.* **2015**, *137*, 7843.
- [53] K. Gauthron, J. S. Lauret, L. Doyennette, G. Lanty, A. Al Choueiry, S. J. Zhang, A. Brehier, L. Largeau, O. Mauguin, J. Bloch, *Opt. Express* **2010**, *18*, 5912.
- [54] P. Lefebvre, P. Christol, H. Mathieu, S. Glutsch, *Phys. Rev. B* **1995**, *52*, 5756.
- [55] L. Ma, J. Dai, X. C. Zeng, *Adv. Energy Mater.* **2017**, *7*, 1601731.
- [56] R. J. Elliott, *Phys. Rev.* **1957**, *108*, 1384.
- [57] A. S. Berestennikov, Y. Li, I. V. Iorsh, A. A. Zakhidov, A. L. Rogach, S. V. Makarov, *Nanoscale* **2019**, *11*, 6747.
- [58] K. He, N. Kumar, L. Zhao, Z. Wang, K. F. Mak, H. Zhao, J. Shan, *Phys. Rev. Lett.* **2014**, *113*, 026803.